We are IntechOpen, the world's leading publisher of Open Access books Built by scientists, for scientists

6,900
Open access books available

186,000
International authors and editors

200M
Downloads

Our authors are among the

154
Countries delivered to

TOP 1%
most cited scientists

12.2%
Contributors from top 500 universities

WEB OF SCIENCE™

Selection of our books indexed in the Book Citation Index in Web of Science™ Core Collection (BKCI)

Interested in publishing with us?
Contact book.department@intechopen.com

Numbers displayed above are based on latest data collected.
For more information visit www.intechopen.com

Chapter 12

Drooped Microstrip Antennas for GPS Marine and Aerospace Navigation

Ken G. Clark, Hussain M. Al-Rizzo,
James M. Tranquilla, Haider Khaleel and
Ayman Abbosh

Additional information is available at the end of the chapter

http://dx.doi.org/10.5772/55002

1. Introduction

The Navigation Satellite Timing and Ranging (NAVSTAR) GPS is a space-based system designed primarily for global real-time, all-weather navigation. There are 30 GPS satellites in six nearly circular, approximately 20,000 kilometer orbital planes, with an inclination of 55^0 relative to the equator [1]. Each satellite transmits two unique, Right Hand Circularly Polarized (RHCP) L band signals. The L1 (1.57542 GHz) carrier is bi-phase modulated with two pseudo-random noise sequences; the P and C/A codes. The L2 (1.2276 GHz) carrier is modulated only with the P code and is used mainly to determine and correct phase advance caused by the ionosphere. Superimposed on the P and C/A codes is the navigation message which contains, among other things, satellite ephemerides, clock biases, and ionosphere correction data [1].

Due to their light weight, reduced size, low cost, conformability, robustness, and ease of integration with MMIC, tremendous research has been reported over the last three decades into the use of microstrip antennas in GPS navigation [2]-[20]. Antenna designers are often faced with interrelated, strict, and conflicting performance requirements in order to meet the accuracy, continuity, and integrity of differential GPS, relative geodetic and hydrographic surveying, ship-borne and aerospace navigation [21]-[27].

The design specifications of a GPS antenna depend on the performance requirements peculiar to the application under consideration. A GPS user antenna requires RHCP and adequate co-polarized radiation pattern coverage over almost the entire upper hemisphere to track all visible satellites. Moreover, the antenna should ideally provide a uniform response in amplitude and, more critically, in phase to the full visible satellite constellation [21]. The angle cutoff

INTECH
open science | open minds

© 2013 Clark et al.; licensee InTech. This is an open access article distributed under the terms of the Creative Commons Attribution License (http://creativecommons.org/licenses/by/3.0), which permits unrestricted use, distribution, and reproduction in any medium, provided the original work is properly cited.

and roll-off characteristics of the radiation pattern can be altered to suit the application of interest. For example, fixed ground reference stations and relative static geodetic surveying demand a rapid fall-off near the horizon, a high cross-polarization rejection, and a front-to-back gain ratio in excess of 20 dB to mitigate deleterious effects of severe multipath [28], [29].

In real-time kinematic positioning, few if any of the above constraints may be effective [30] and it may be necessary to operate the antenna under less than optimal conditions in regard to cross polarization performance if a wide beamwidth is of precedence. Precise GPS hydrographic surveying on a vessel cruising at speeds of 10 to 20 knots in open oceans is a challenging task due to the rotational disturbances from a relatively harsh sea environment. Pitch and roll amplitudes as high as 10^0 to 15^0 may be encountered in stormy weather, which presents a major obstacle to GPS derived attitude determination [21], [22]. Another envisaged application for the drooped microstrip antennas introduced in this chapter involves normal pitch or roll maneuvers of a general aviation aircraft, which may cause loss of some satellite signals for a range of flight orientation.

There is significant interest in the commercial and military sectors to develop antennas that could cover much of the upper hemisphere, including GPS satellites at elevation angles as low as 10^0, and to extend the coverage to negative elevation angles [3], [4], [15], [21]. This will lead to fewer occurrences of cycle slips and loss of lock to satellites while rising or setting, will maintain the proper Dilution of Precision (DoP) by maximizing the number of satellites in view, and will reduce the RMS error in range and velocity [1]. Notably, on the negative side, undesired multipath reflections off water and conducting bodies are also strongest at low-elevation angles. Nevertheless, whatever type of antenna is chosen, multipath reception will still have to be dealt with as a common problem [30]. It is fair to say that no single antenna design in the open literature has satisfactorily fulfilled all the above-mentioned requirements on coverage, phase center stability, and multipath rejection for real-time highly dynamic GPS marine and aerospace applications.

A pedestal ground plane is reported in [31], based on a trial-and-error experimental design approach, consisting of a cylindrical structure with a flat elevated center surrounded by sloping sides, to address beam shaping of crossed dipoles. This structure was found to be successful in improving the pattern coverage of the crossed dipole at low-elevation angles. Additional elements were also examined such as folded, serrated, rolled edges, monofilar, and quadrafiliar helices [32]-[35], although none achieved the same degree of radiation pattern control as the crossed dipole. This is attributed in part to the extent of ground plane illumination produced by the different sources and serves to highlight the importance of the ground plane as a secondary source with which to produce pattern changes. Further modifications to the ground plane using choke rings [28] were investigated primarily for multipath rejection.

It is well known that a stand-alone microstrip antenna mounted on a flat ground plane suffers from a lack of pattern control and reduced gain at low-elevation angles. This may result in a loss of contact with satellites when the antenna is mounted on a highly-dynamic platform, an attractive use for this low-profile structure. Fundamental to the design of a patch antenna is the interaction with the ground plane. In fact, the size, orientation, and shape of the ground plane are among the most important parameters that have an influence on the radiation pattern

http://dx.doi.org/10.5772/55002

[36]. However, a fundamental distinction exists in the relationship between a patch and the ground plane when compared with helical or dipole elements in that the ground plane of a microstrip antenna forms an integral part of the radiating structure and may not best be defined as a "secondary" source.

Building on our previous design experiences [28], [31]-[35], our research group at the University of New Brunswick, Fredericton, NB, Canada was the first to rigorously investigate the potential performance enhancements and limitations involved when these design modifications are applied to the more appealing microstrip antenna element [37]. The advantages associated with the microstrip antenna are such that one patent has been issued to a GPS manufacturer [38] based only on a downward drooped antenna structure. Neither the dimensions nor the performance of the proposed antennas were quantified in [38]. Later, a corner truncated square patch, partially enclosed within a flatly folded conducting wall, mounted on a pyramidal ground plane, was reported in [39]. However, neither the cross polarization performance nor the phase center stability were provided in [39].

In contrast to the antenna reported in [39], the drooped microstrip antennas introduced in this chapter have the ground plane and actual element deformed such that the corners or edges of the resonant cavity region fall away from the plane occupied by the element. A fundamental understanding of the operation and limitations of the drooped microstrip antenna is still lacking. A diffraction technique was attempted in [40] to model the effects of a sloping ground plane. This, however, was limited by the difficulty of implementing a realistic source term as well as the inclusion of finite lossy dielectric materials. A rigorous full-wave 3-D model, which incorporates the coaxial feed and detailed geometrical features of the drooped microstrip antenna, has not yet been reported.

For these reasons, we have performed the research reported in this chapter, which is the first to our knowledge that combines rigorous 3-D full-wave simulations and experimental measurements to provide a comprehensive characterization of downward and upward drooped microstrip antennas. A FDTD model has been developed, validated experimentally, and used to compute the input impedance and far-field radiation patterns. The FDTD model was used to examine the effects of a wide range of structural variations to gain an insight into the benefits and limitations of the proposed antennas. The parameters of interest include the location and angle of the bend, length of the ground plane, dielectric constant, and thickness of the substrate. Prototype structures were constructed, and their characteristics measured and then compared against simulated results. The authors wish to point out that the antennas described in this chapter are not intended to target multipath mitigation; on the contrary, they demonstrate the range of pattern modifications that could be accomplished by manipulating the orientation and size of the ground plane to suit GPS applications in marine and aerospace navigation.

The rest of the chapter is organized as follows: Section 2 summarizes the FDTD algorithm developed to perform the design and parametric studies and presents results from experimental tests performed to validate the implementation of the model and to demonstrate its ability to correctly predict the behavior of the drooped antennas. Section 3 addresses the design procedure, introduces parametric studies, and describes the drooped antennas constructed and tested for the control of the radiation patterns. Finally, Section 4 provides concluding remarks.

2. The contour path FDTD model: Experimental validation

The basic microstrip antenna, which consists of a conducting patch radiator rotated by 45^0 with respect to the center of the ground plane, and separated from the ground plane by a thin dielectric substrate, and the downward drooped antenna are shown in Figure1.

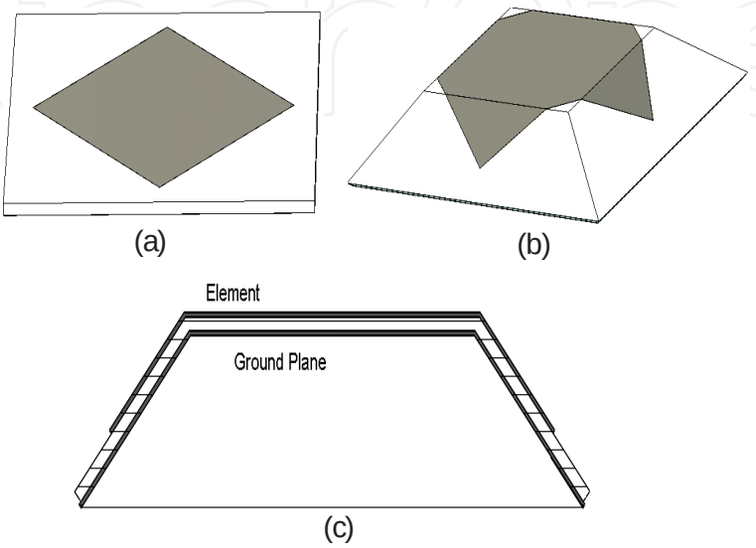

Figure 1. (a) The reference flat microstrip antenna, (b) the downward geometry, (c) cross sectional view of the resonant cavity.

The element is driven by a 50 Ω coaxial cable passing through the ground plane and the substrate. The antenna operates at the L1 GPS frequency of 1.57542 GHz since the majority of commercial GPS receivers use only the L1 frequency. Due to the relatively low cost, time savings, and repeatability, computer simulations can often complement and reduce the empiricism involved in an otherwise purely experimental approach, particularly in the initial design phase, allowing the antennas to be characterized carefully prior to their construction. Because of the complex geometries involved, the task of modeling the drooped microstrip structures is by no means a simple endeavor; it better lends itself to numerical simulation techniques. The FDTD method has been adopted in this research due to its conceptual simplicity and ease of implementation. Because it is a time-domain scheme, it is straightforward to impose a pulse excitation to perform broadband analysis using the Discrete Fourier Transform (DFT).

The FDTD algorithm is implemented in a 3-D Cartesian coordinate system with the formulation allowing for different spatial increments along each coordinate direction. Provision is made for modeling symmetrical objects by applying the Neumann boundary condition along one surface of the computational space. The antenna is excited either by a sinusoidal signal at the resonant frequency of the dominant mode or by a Gaussian pulse with a specified width and delay. The excitation is applied to either the electric or magnetic field, depending on whether a voltage or current source is desired.

http://dx.doi.org/10.5772/55002

In order to compute the input impedance, the instantaneous voltage and current are calculated at a fixed location in the coaxial feed by integrating the radial electric field and the magnetic field components encircling the inner conductor of the coaxial cable. A Gaussian pulse is used, and a DFT is performed to obtain broadband results. The impedance is then translated into the ground plane aperture by standard transmission line methods. The far-field radiation patterns are next determined by driving the model to steady state, using a sinusoidal wave at the fundamental resonant frequency of the antenna.

With pulse excitation, the fields must settle toward zero as energy escapes through the absorbing boundary. The condition used to judge if steady state is reached requires that the energy monitored at several observation points within the computational domain remains below 1% of the peak observed value with lower values enforced for cases continuing to display periodic oscillations in the fields. For a sinusoidal excitation, the solution must converge to an oscillation. The magnitude and phase at several observation points are extracted from the DFT at each temporal cycle. A 1% variation in steady state is permitted in phase.

The methodology we followed involves extracting the antenna characteristics for a given geometry selected from a parametric study using the FDTD code; constructing a prototype; measuring the frequency response of the input impedance, far-field radiation patterns at the measured resonant frequency; and finally comparing simulated results against measurements. To validate the operation of the FDTD model, several antenna structures were simulated and measured. The first antenna used to validate the code was a flat rectangular microstrip. The 50 mm × 47 mm patch was constructed on a square ground plane, 150 mm in side length. The substrate has a relative dielectric constant, ε_r = 4.2 and a thickness of 1.5 mm. The frequency spectrum of the real and imaginary parts of the input impedance and the far-field radiation pattern in the *E* plane are shown in Figs. 2 and 3, respectively.

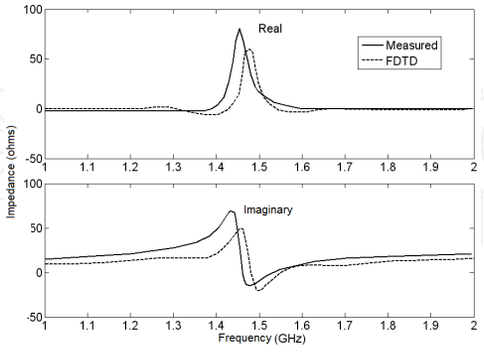

Figure 2. Measured and calculated input impedance for a 50 mm × 47 mm microstrip on a flat, 150 mm square ground plane.

The calculated impedance correctly predicts the resonant frequency measured using a network analyzer. Similarly, excellent agreement is observed between the amplitude and phase of the measured and simulated far-field radiation patterns.

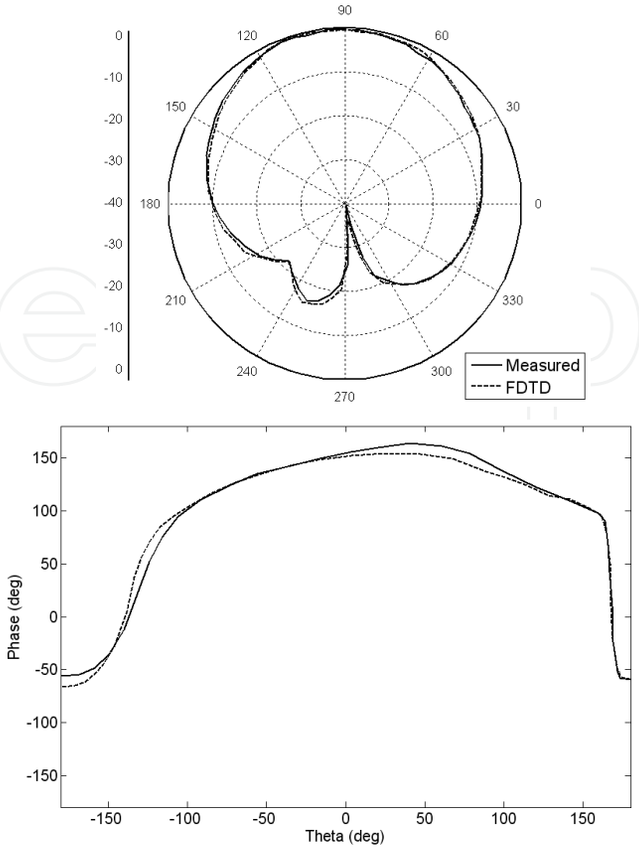

Figure 3. Normalized amplitude and phase of the far-field radiation pattern in the *E* plane for a 50 mm × 47 mm flat microstrip on a 150 mm square ground plane.

As a progression toward the drooped structure, a microstrip antenna with two edges bent down at an angle of 45^0 was modeled. This structure requires special consideration in that the boundary conditions imposed by the element and ground plane do not fall along the coordinate planes. The most straightforward approach is to discretize the sloping sides with the traditional stair-stepped approximation. However, it has been observed that this can result in a slight change in the resonant frequency of high *Q* structures [41]. To avoid errors associated with the conventional FDTD method, we used the contour path method introduced in [42]. In this approach, a field component adjacent to a boundary is not updated in terms of the spatial derivatives of the surrounding fields but by an integration of adjacent fields along the perimeter of the cell. This allows for partial or deformed cells, thus better approximating the drooped surfaces.

Three different step approximations, shown in Figure 4, were used to model the sloping sides, depending upon the angle of the bend. *For fine adjustments*, the ratio of the vertical to horizontal spatial increments is adjusted to yield the desired slope angle. This has an additional benefit of simplifying the implementation of the contour method when applied to field components adjacent to the sloped surfaces. Because each cell is truncated in the same way, the contour corrections proceeded without the need to calculate intercepts of the actual slope line at each cell.

http://dx.doi.org/10.5772/55002

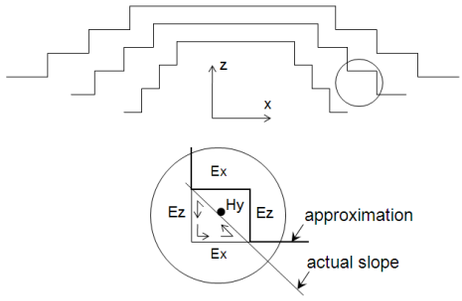

Figure 4. Stepped approximation of shallow, intermediate, and steep bend angles. Fine adjustments are made by varying the $\Delta x/\Delta z$ ratio. The contour integral correction is made to adjacent H fields to define the actual surface.

A rectangular microstrip with two 45^0 drooped edges fed by a coaxial cable was constructed and tested to compare measured and simulated input impedance, E and H plane patterns. The geometry of the antenna is shown in Figure 5 along with the phase of the E plane elevation cut. The measured phase displayed in Figure 5 showed a slight asymmetry due to the offset in antenna mount necessary to accommodate the bends and the connector. For comparison, we referenced the calculated far-field patterns to the same offset origin. The E plane and H plane patterns shown in Figs. 5 and 6 along with the impedance of Figure 7 reveal good correspondences between measured and simulated results.

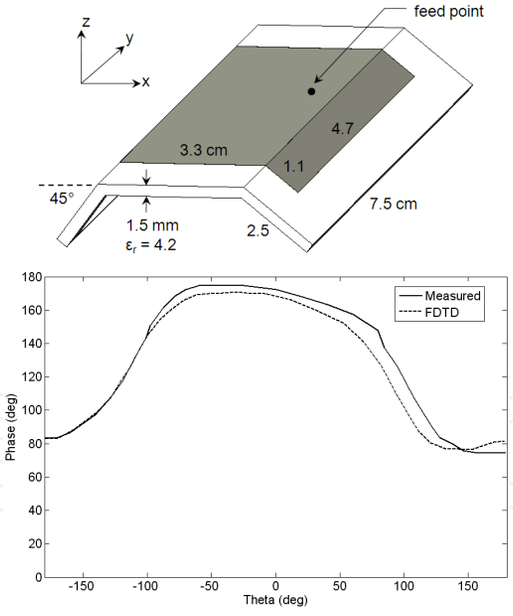

Figure 5. E plane (x-z plane) elevation phase for a 55 mm × 47 mm microstrip with a 45° bend, centered on a 83 mm × 75 mm ground plane.

Before progressing to the double-bend antenna, a test was conducted to verify that the FDTD model maintained continuity at the point where the stepped approximation changed from a 2:1 to a 1:1 ratio. To accomplish this, we modeled a 40 mm × 50 mm bent microstrip antenna near the change of an angle of 55^0 using both ratios. A comparison of the input impedance and

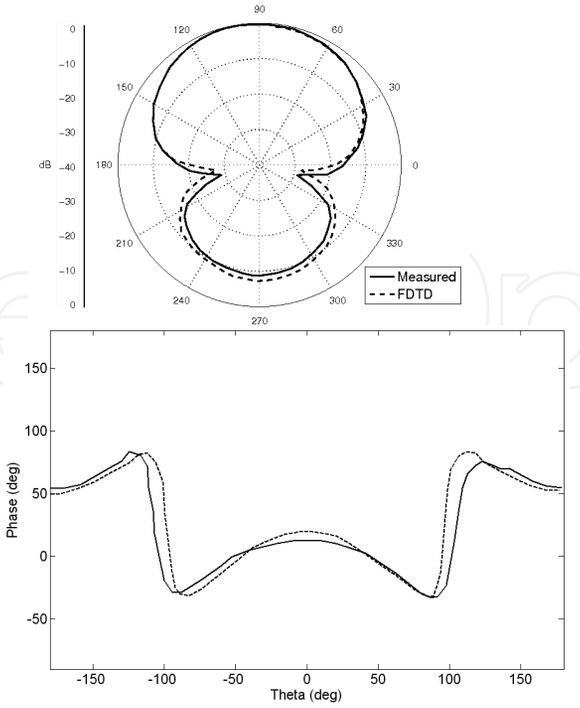

Figure 6. *H* plane elevation pattern for a 55 mm × 47 mm microstrip with a 45° bend, 10 mm from each short side, magnitude (top) and phase (bottom).

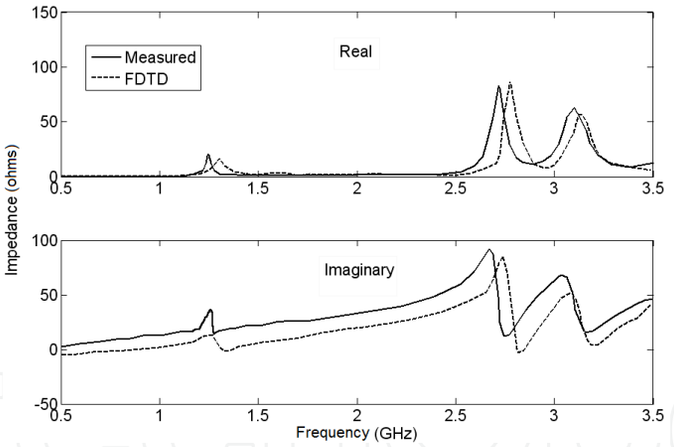

Figure 7. Measured and calculated input impedance for a 47 mm × 55 mm microstrip on a 45° bent ground plane (33 mm flat top with 11 mm bent over each angle).

elevation patterns depicted in Figure 8 show good agreement between results obtained from each approximation.

To duplicate the bend on the two remaining sides to achieve the full drooped structure, we constructed two drooped antennas and used them to verify the performance of the completed model. The first antenna, shown in Figure 9, consists of a 62 mm × 62 mm patch, a 40 mm square elevated section, printed on a 1.5 mm thick substrate, $\varepsilon_r = 4.2$, and a 60^0 droop angle. The second is a 64 mm × 64 mm patch, a 50 mm square elevated section, printed on a 3 mm

http://dx.doi.org/10.5772/55002

substrate, ε_r = 2.2, and a 30^0 droop angle. Results obtained for the real and imaginary parts of the input impedance and far-field radiations patterns, as shown in Figs. 9 and 10, respectively, display good agreement between simulated and measured results. The excellent agreement demonstrated thus far between the amplitude and phase of the simulated and measured far-field radiation patterns prompted further exploration of the possibility of controlling the radiation pattern by manipulating the droop parameters.

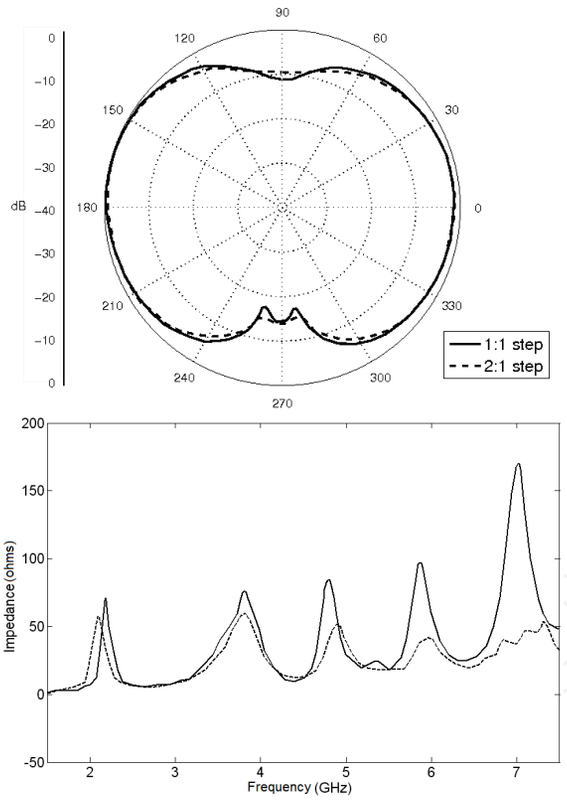

Figure 8. *E* plane pattern and impedance comparison for 50 mm × 40 mm microstrip (ε_r = 2) with a 55° bend, calculated for a 1:1 and 2:1 step approximation of the sloped sides.

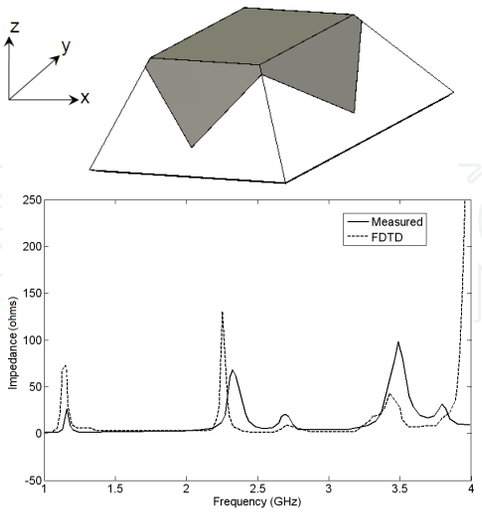

Figure 9. Measured and calculated input impedance for a 60° double bend microstrip.

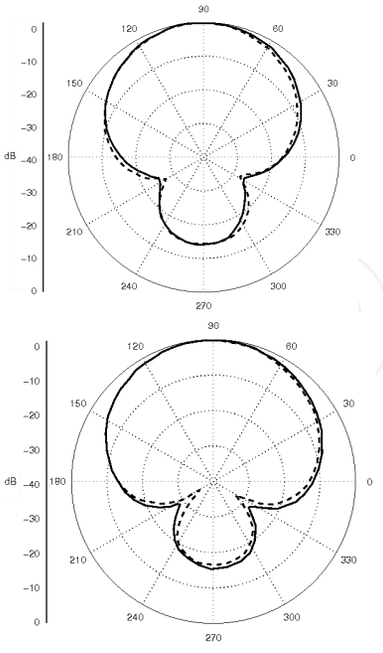

Figure 10. Measured and calculated elevation patterns for 64 mm square microstrip with a 30^0 bend, $\varepsilon_r = 2.2$, *E* plane (*x*-*z*) top and *H* plane (*y*-*z*) bottom (1550 MHz).

http://dx.doi.org/10.5772/55002

3. Parametric analysis of the drooped microstrip antennas

Further parametric analyses were conducted to determine the range of structural variations that can be utilized to optimize the performance of the drooped microstrip antennas. The design process was complicated due to the several interacting parameters that must be considered in order to provide adequate low-angle coverage, uniform phase response, and polarization purity. Parameters investigated include the angle and location of the bend, length of the ground plane skirt, thickness and dielectric constant of the substrate. The results are assessed on the basis of their impact on antenna gain at bore sight, phase performance in the upper hemisphere, pattern beamwidth, cross polarization rejection, and near horizon gain reduction.

In all cases to be presented, the radiation patterns were obtained at the resonant frequency of the dominant mode. The amplitude and phase of the radiation patterns were obtained from anechoic chamber measurements in a $5^0 \times 5^0$ grid, following the procedure described in [43]. These were then analyzed to determine the 3 dB beamwidth and near horizon gain reduction with respect to bore sight (zenith). In order to determine the absolute gain, we integrated the calculated patterns over the upper and lower hemispheres with a 5^0 step in azimuth and elevation. All field calculations were then referenced to the resulting isotropic power density.

Whereas an enormous volume of literature is available on patch antennas for GPS applications [2]-[20], a close scrutiny revealed that the design objectives in the majority of these studies and the performance characterization were based entirely on the amplitude of the co- and cross-polarized radiation patterns. Only few have considered the phase response as a figure of merit in the design process and/or in the analysis or measurements [28], [31]-[35], [43]. The phase response directly weighs the arriving signals and produces a phase-shaping effect, which depends on the angle of arrival of the satellite signals. The calibration of the phase response provides invaluable information regarding the level of accuracy one can ultimately achieve for sub-centimeter static geodetic positions [43].

The measured upper hemispherical phase response of the antennas under test was matched to an ideal hemisphere in a $5^0 \times 5^0$ grid, using equal solid angle weighting. The position of the ideal hemisphere was adjusted to minimize the RMS error between the measured and ideal phase [43]. The origin of this hemisphere is defined as the "center of best fit" or "phase center," and the difference between the measured and ideal phase is defined as the "phase residual" or "phase error." The RMS value of the phase error is used as a figure of merit to describe the phase distortion introduced by the antennas considered in the rest of this chapter.

3.1. Drooped microstrip with a downward bend

For the initial test, a 40 mm × 40 mm patch was placed on three different ground planes. These, in turn, were bent at three different distances from the center, forming a flat square top that was 10, 30, or 50 mm^2. Simulations were carried out for bend angles, ranging from 0 to 90^0 in a 15^0 step. Figure 11 depicts the parameters and geometries used for the initial set of simulations.

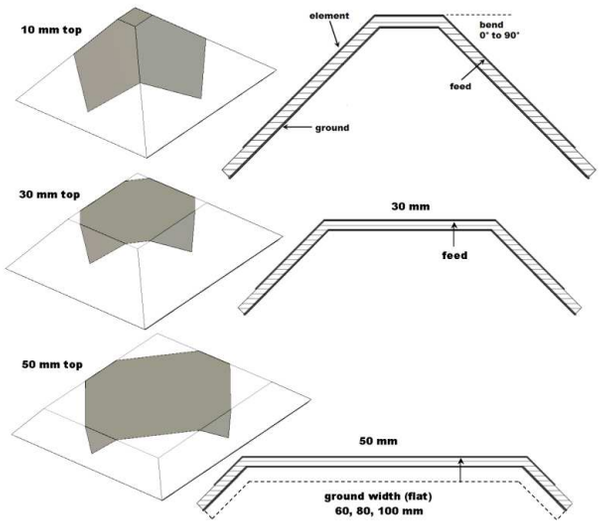

Figure 11. Initial structural variations included three bend locations at 5, 10, and 25 mm from the patch center, droop angles ranging from 0° to 90° and 3 ground planes having flat (unbent) dimensions of 60, 80, 100 mm. Three substrate materials with relative permittivity of 2.2, 4.2, and 10.

Three dielectric constants were used in the course of the simulations to examine the effects of different substrate materials; values of 2.2 and 4.2 were selected because of the availability of substrates to construct the verification cases, while an ε_r of 10 was chosen as an example of a ceramic substrate frequently used in industry. Copper tape applied to bulk Teflon, one eighth inch thick, was used to form several fixed and adjustable structures. A standard polyester-based circuit board was used to construct others.

A sequence of elevation patterns is presented in Figure 12, which displays the progression of the radiated fields with the size and bend angle of the ground plane. Not unexpectedly, smaller ground planes with larger bends allow more energy to escape off the back, until it appears that the main beam is 180^0 from the bore sight direction. This is made obvious by plotting the polar patterns for E_θ, using a linearly polarized excitation. With a circularly polarized excitation, backward radiated energy appears predominately in the cross polarized component, making the effect less noticeable. Notably, all subsequent results for gain, beamwidth, or phase are presented while exciting circular polarization as this would be the normal operating mode of the antenna.

http://dx.doi.org/10.5772/55002

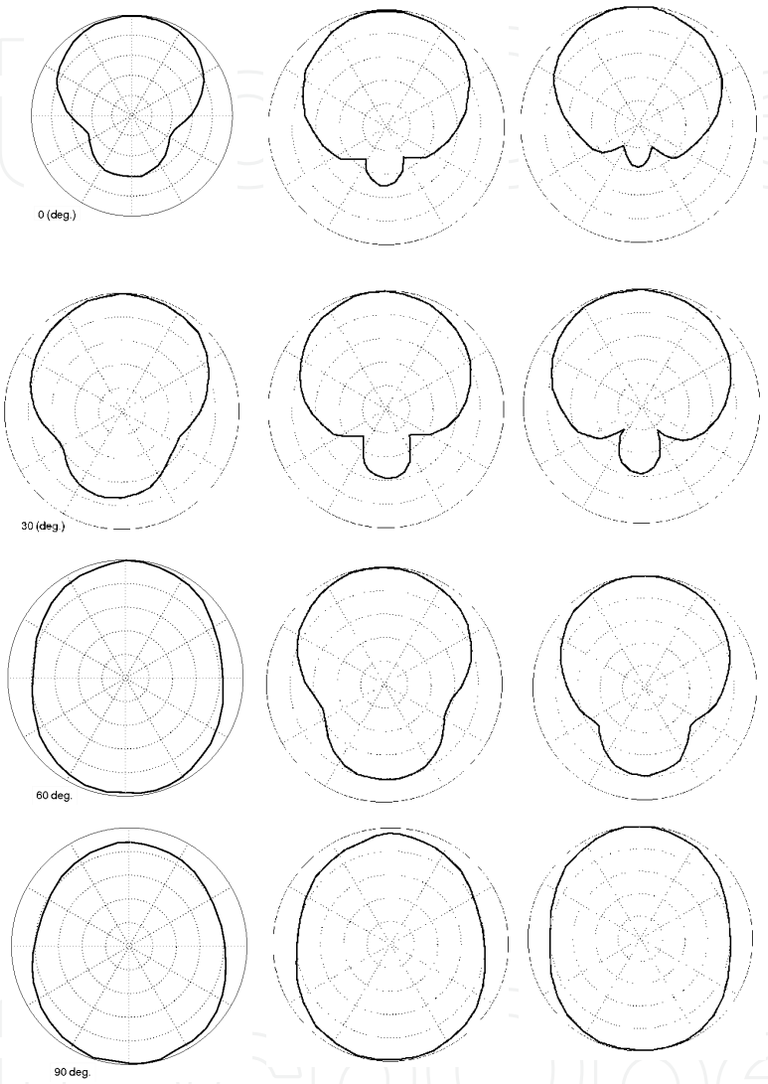

Figure 12. Elevation patterns for bend angle variations of 0° to 90° with 60 (left), 80 (center), and 100 (right) mm ground planes. E_θ component, $\varepsilon_r = 2.2$, all with 30 mm top. All patterns are normalized to 0 dB maximum, 10 dB/division.

Next, a prototype was constructed with adjustable bend plates, and the measured beamwidths were compared against simulated results. For construction simplicity, the antenna was excited using linear polarization with only two sloped sides. In Figure 13, the measured and computed beamwidths show a slight improvement with increasing bend angle.

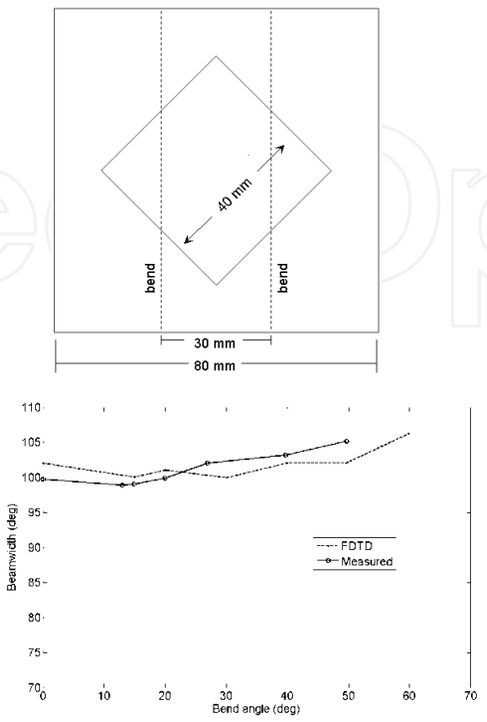

Figure 13. Measured and computed 3 dB beamwidth for an adjustable bend microstrip antenna.

Variations in bore sight gain, 3 dB beamwidth, near-horizon gain roll-off, and RMS phase error as a result of increasing the bend angle are summarized in Tables 1 to 3. The 10 mm case shows a sharp gain reduction at extreme bend angles. The results reveal a relatively minor improvement in the pattern beamwidth, even for large bend angles and varying ground plane sizes for the higher dielectric substrates. Indeed, the radiation patterns above the horizon remain virtually unchanged for bend angles up to 60^0.

ε_r=2.2		Boresight gain (dBi)			3 dB Beamwidth (deg)			Near horizon gain Roll-off (dB)			RMS phase error (deg)		
Width-mm		60	80	100	60	80	100	60	80	100	60	80	100
Bend angle (10 mm top)	0	7.2	7.5	7.7	88	83	80	-11.	-12.	-13.	3.0	2.6	2.0
	15	7.1	7.5	7.7	88	84	80	-10.	-11.	-13.	2.5	3.3	3.4
	30	6.9	7.1	7.1	90	86	86	-9.7	-10.	-11.	1.5	1.8	1.7
	45	5.5	6.5	6.4	96	95	96	-9.0	-9.1	-9.1	2.2	1.6	2.0
	60	0.9	5.6	6.2	100	94	97	-7.9	-9.5	-9.0	4.3	6.5	2.6
	70	0.8	3.3	5.4	119	91	95	-5.5	-9.3	-9.0	12.	4.4	2.8
	90	-24	-25	-26	354	356	356	22	23	24	11.9	2.7	2.8

http://dx.doi.org/10.5772/55002

ε_r=2.2		Boresight gain (dBi)			3 dB Beamwidth (deg)			Near horizon gain Roll-off (dB)			RMS phase error (deg)		
Width-mm		60	80	100	60	80	100	60	80	100	60	80	100
Bend angle (30 mm top)	0	7.2	7.5	7.7	88	83	80	-11.	-12.	-13.	2.9	2.6	2.0
	15	7.1	7.5	7.8	88	83	78	-11.	-11.	-13.	2.4	3.3	3.4
	30	6.9	7.4	7.4	89	83	82	-9.6	-11.	-11.	1.5	1.8	1.7
	45	6.6	7.1	7.0	90	87	87	-10.	-10.	-11.	1.9	1.6	2.0
	60	5.5	6.7	6.5	91	90	93	-10.	-10.	-9.7	2.3	6.5	2.6
	70	5.2	6.4	6.2	92	92	96	-10.	-9.9	-9.1	1.6	4.4	2.8
	90	0.1	2.3	3.78	97	84	85	-9.6	-11	-12	8.2	2.7	2.8
Bend angle (50 mm top)	0	7.2	7.5	7.7	88	83	80	-11.	-12.	-13.	2.9	2.6	2.0
	15	7.0	7.7	7.9	89	81	77	-10.	-12.	-13.	2.4	3.3	3.4
	30	7.1	7.5	7.4	87	82	83	-9.9	-11.	-11.	1.5	1.8	1.7
	45	6.9	7.2	7.1	89	86	87	-9.6	-10.	-10.	1.9	1.6	2.0
	60	6.8	7.2	7.0	89	87	88	-9.7	-10.	-10.	2.3	6.5	2.6
	70	7.1	7.2	6.8	87	87	91	-10.	-10.	-9.4	1.6	4.4	2.8
	90	6.4	6.9	6.9	91	89	89	-9.4	-9.7	-10.	8.2	2.7	2.8

Table 1. Results for the drooped microstrip, substrate permittivity 2.2.

ε_r=4.2		Boresight gain (dBi)			3 dB Beamwidth (deg)			Near horizon gain Roll-off (dB)			RMS phase error (deg)		
Width-mm		60	80	100	60	80	100	60	80	100	60	80	100
Bend angle (10 mm top)	0	4.7	5.8	6.2	106	100	100	-11.6	-13.5	-14.5	1.6	1.2	1.1
	15	4.5	5.7	6.0	106	103	100	-9.9	-10.8	-10.9	2.2	3.6	4.3
	30	4.8	5.9	6.0	106	100	101	-8.6	-11.0	-10.7	1.5	1.0	1.0
	45	3.4	5.2	6.5	149	107	108	-3.7	-9.0	-9.7	2.0	1.5	1.2
	60	0.9	4.3	6.1	360	129	115	2.5	-5.7	-8.4	3.6	2.7	2.6
	70	-1.1	1.5	3.3	360	360	144	6.5	0.8	-3.8	12.8	2.9	3.3
	90	-27	-28	-29	360	360	360	-	-	-	-	-	-
Bend angle (30 mm top)	0	4.7	5.8	6.2	114	106	100	-11.6	-13.5	-14.5	1.6	1.2	1.1
	15	4.5	6.0	6.0	119	103	103	-10.6	-13.8	-13.7	1.2	1.1	0.9
	30	4.6	5.9	6.0	113	104	102	-11.1	-13.3	-13.5	0.9	0.5	0.5
	45	4.9	5.8	5.9	107	104	106	-12.2	-13.4	-13.4	1.2	0.8	0.7
	60	3.5	4.4	5.3	106	109	112	-11.3	-11.4	-12.0	1.6	1.9	1.3
	70	3.0	4.3	4.8	116	114	115	-9.2	-10.9	-11.3	0.9	0.9	0.8
	90	1.0	1.5	2.4	121	110	103	-6.7	-8.2	-10.1	1.6	1.5	1.4

ε_r=4.2		Boresight gain (dBi)			3 dB Beamwidth (deg)			Near horizon gain Roll-off (dB)			RMS phase error (deg)		
Width-mm		60	80	100	60	80	100	60	80	100	60	80	100
Bend angle (50 mm top)	0	4.8	5.8	6.2	114	106	100	-11.6	-13.5	-14.5	0.8	0.9	1.2
	15	4.9	5.9	6.3	119	103	103	-11.5	-13.6	-14.6	0.7	0.7	0.9
	30	5.3	6.0	6.2	113	104	102	-12.5	-13.6	-14.1	0.6	0.5	0.6
	45	5.0	5.8	6.0	107	104	106	-12.4	-13.4	-13.4	0.7	0.6	0.6
	60	4.7	5.6	5.8	106	109	112	-11.7	-12.8	-13.3	0.6	0.6	1.0
	70	5.2	5.5	5.4	116	114	115	-12.2	-12.5	-12.0	0.4	0.4	0.5
	90	4.4	5.2	5.4	121	110	103	-11.6	-12.6	-12.8	0.8	0.6	0.6

Table 2. Results for the drooped microstrip, substrate permittivity 4.2.

ε_r=10		Boresight gain (dBi)			3 dB Beamwidth (deg)			Near horizon gain Roll-off (dB)			RMS phase error (deg)		
Width-mm		60	80	100	60	80	100	60	80	100	60	80	100
Bend angle (10 mm top)	0	3.1	4.7	5.3	114	108	104	-9.4	-11.5	-12.5	0.80	0.49	0.53
	15	3.4	4.4	5.2	116	115	111	-9.3	-10.4	-11.4	0.89	1.0	0.87
	30	3.8	4.4	5.1	117	113	111	-9.7	-10.7	-11.3	0.59	0.46	0.42
	45	2.5	3.6	4.5	123	117	116	-7.8	-9.5	-10.6	0.41	0.41	0.38
	60	3.3	2.6	3.6	139	120	118	-8.2	-8.3	-9.5	3.0	0.80	0.86
	70	2.4	3.0	3.5	134	122	120	-7.4	-8.5	-9.3	2.0	0.72	0.97
	90	-38	-40	-43	360	360	360	-	-	-	-	-	-
Bend angle (30 mm top)	0	3.1	4.7	5.3	114	108	104	-9.4	-11.5	-12.5	0.80	0.49	0.53
	15	3.8	4.5	4.9	119	108	106	-9.6	-11.3	-11.9	0.40	0.46	0.48
	30	3.8	5.0	5.4	116	106	106	-9.8	-12.1	-12.5	0.25	0.33	0.36
	45	2.9	4.1	4.7	116	114	114	-8.9	-10.3	-10.9	0.39	0.32	0.30
	60	2.7	3.6	4.3	119	104	104	-8.6	-11.1	-12.0	0.56	1.2	1.2
	70	2.3	2.9	3.5	122	119	119	-7.8	-8.6	-9.3	0.24	0.21	0.18
	90	1.5	1.4	1.5	134	132	127	-6.0	-6.1	-6.6	0.29	0.31	0.34
Bend angle (50 mm top)	0	3.1	4.7	5.3	114	108	104	-9.4	-11.5	-12.5	0.80	0.49	.53
	15	2.9	4.6	5.4	133	114	109	-7.6	-10.7	-11.7	0.34	0.70	0.80
	30	3.2	4.9	5.5	121	110	109	-8.7	-12.4	-11.8	0.46	0.90	0.32
	45	3.4	4.5	4.8	119	112	117	-9.0	-10.7	-10.4	0.37	0.56	0.41
	60	3.0	3.7	4.9	122	124	119	-8.4	-8.9	-11.8	0.51	0.51	0.90
	70	3.7	3.6	4.5	117	123	107	-9.5	-9.1	-10.3	0.28	2.2	1.5
	90	2.0	2.6	3.2	113	110	108	-8.3	-9.2	-10.0	2.1	2.4	2.2

Table 3. Results for the drooped microstrip, substrate permittivity 10.

http://dx.doi.org/10.5772/55002

The phase of the elevation cuts shown in Figure 14 shows a remarkable change in the below-horizon phase. For small bend angles, the phase diminishes from the bore sight value when approaching the horizon, while at higher bends the phase increases from the bore sight value. At about 15^0 to 30^0 of bend, a region exists where the elevation phase remains relatively constant above the horizon. Bending of the structure in this manner could provide an additional beamwidth and, more importantly, the phase stability necessary to achieve a design specification, particularly if further modification of the substrate is not feasible.

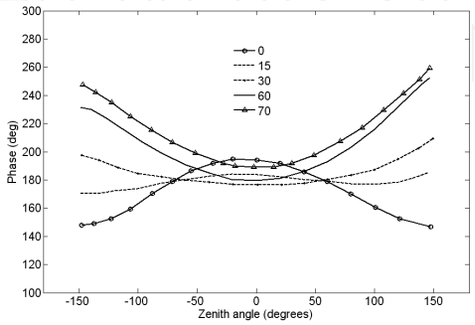

Figure 14. Elevation phase patterns for different bend angles (0^0, 15^0, 30^0, 60^0, and 70^0), with a 100 mm ground plane and a 30 mm flat ($\varepsilon_r = 4.2$).

Another consideration for GPS antennas is the cross polarization behavior. Odd reflections from nearby objects tend to be orthogonally polarized. Hence, it is important that the antenna be able to reject these, particularly near the horizon. To demonstrate the effect of bending the structure on the polarization performance, we examined the ratio of the right- to the left-hand

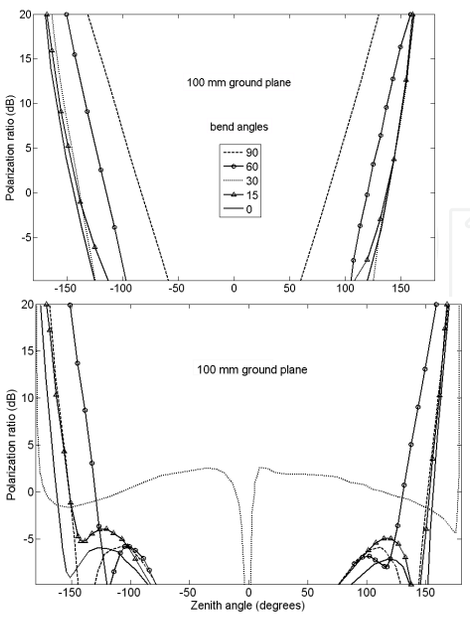

Figure 15. Cross polarization rejection (Defined as the ratio of the cross-polarized to the co-polarized components) for different bend angles (0^0, 15^0, 30^0, 60^0, and 90^0); top, $\varepsilon_r = 4.2$, bottom, $\varepsilon_r = 2.2$.

circular components for several bend angles. Almost without exception, the bend degraded the cross polarization rejection near the horizon as shown in Figure 15, making the antenna more susceptible to spurious signals.

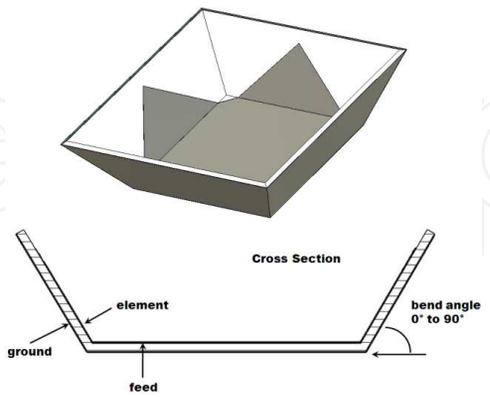

Figure 16. Geometry of the upward bend antenna.

3.2. Drooped microstrip with an upward bend

The modification of the FDTD model to accommodate upward bends was accomplished by interchanging the positions of the ground plane and the element. The structure would then be upside down in the computational space but would have an upward bend. Initially, we considered the antenna shown in Figure16, which has a 30 mm flat top on a substrate with ε_r = 2.2. Three ground plane sizes were analyzed with bend angles varied up to 90^0. Figure 17

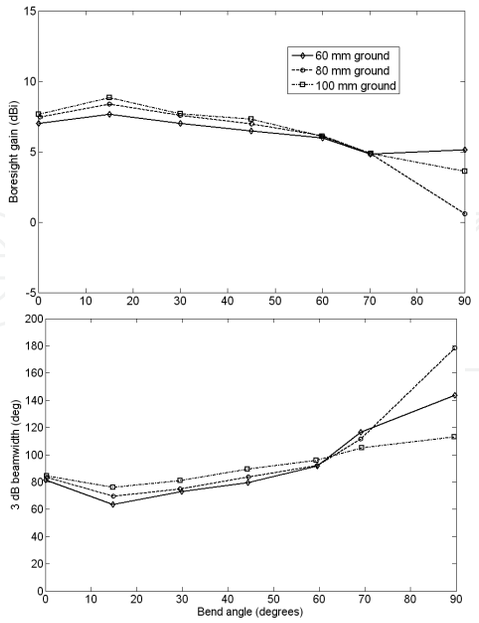

Figure 17. Gain and beam width variation with upward bend angle for three ground plane sizes, ε_r = 2.2. (Bend forming a 30 mm flat center section).

http://dx.doi.org/10.5772/55002

shows the gain and the 3-dB beamwidth for the upward bend cases. As seen, a noticeable beam broadening is evident at the higher bend angles with 3-dB beamwidths up to 60% greater than the equivalent flat case. One can observe, however, a distinct reduction in the beamwidth for the initial small bend angles, particularly for larger ground planes. The beamwidth did not recover to that of the equivalent downward case until the bend angle exceeded 60^0.

A prototype antenna was constructed and tested to allow comparison against experimental results. The antenna is identical to the one shown in Figure 13; only two variable upward bends were used in this case. For measurement purposes, a linearly polarized excitation was used. The initial dip in the beamwidth did not occur in the simulated and measured results shown in Fig. 18.

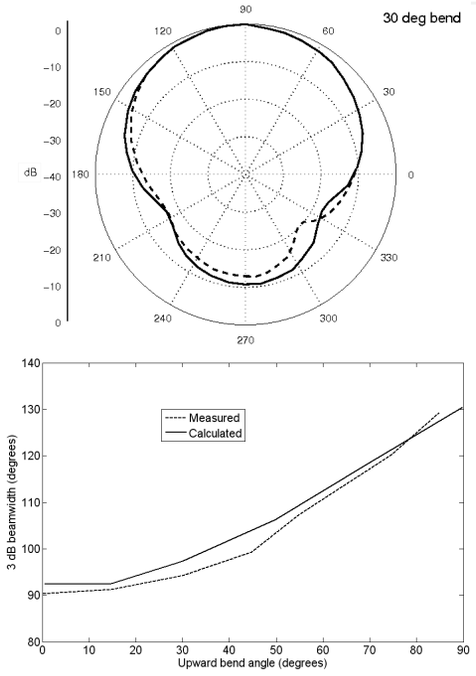

Figure 18. *E* plane elevation pattern and beamwidth behavior of the adjustable upward bend antenna.

With the completion of the initial set of simulations and measurements, we pursued the model with additional parameter variations. Bend locations at the 10 and 50 mm positions were tested for the $\varepsilon_r = 2.2$ substrate. Also, the $\varepsilon_r = 4.2$ substrate was examined when the bend was positioned at the 30 mm position. The results are summarized in Tables 4 and 5.

A changing upward bend produced little effect on the phase in the upper hemisphere. All phase curves above 90^0 elevation fell within 30^0 of each other over the full range of bend angles. Like the downward bend, the RMS phase error over the hemisphere did not vary substantially with bend angle, although a slightly greater differentiation is evident between different ground plane sizes. The elevation gain and cross polarization rejection for various upward bend angles are displayed in Figs. 19 and 20, respectively. When compared to Figure 15, it is apparent that the rejection is better by 2 dB near the horizon for upward bends, but the opposite is true below the horizon. In both cases, bending the ground plane reduces the cross-polarization discrimination near the horizon.

ε_r=2.2		Boresight gain (dBi)			3 dB Beamwidth (deg)			Near horizon gain Roll-off (dB)			RMS phase error (deg)		
Width-mm		60	80	100	60	80	100	60	80	100	60	80	100
Bend angle (10 mm top)	0	7.2	7.5	7.7	88	83	80	-11.	-12.	-13.	3.0	2.6	2.0
	15	4.0	6.2	6.4	158	134	118	-14.	-11.	-11.	6.2	6.8	9.1
	30	4.7	6.5	1.3	143	122	120	-9.4	-10.	-12.	3.6	3.5	5.5
	45	5.1	3.5	3.5	137	170	106	-7.2	-7.6	-9.4	4.5	3.3	3.3
	60	4.1	-.8	2.6	142	302	214	-3.8	-6.7	-7.1	6.6	5.2	4.6
	70	2.5	-4.4	-.42	127	327	300	0.44	5.8	5.7	35.8	6.5	11.2
	90	-1.5	-6.1	-6.4	188	360	360	-2.3	-6.6	0.93	11.0	69.9	80.1
Bend angle (30 mm top)	0	7.2	7.5	7.7	88	83	80	-11.	-12.	-13.	3.0	2.6	2.0
	15	7.7	8.4	8.7	75	69	63	-12.	-13.	-15.	1.8	1.6	3.9
	30	7.1	7.6	7.7	81	75	73	-11.	-12.	-13.	2.8	2.4	4.0
	45	6.6	7.0	7.3	89	83	79	-9.1	-9.8	-11.	2.3	1.5	2.0
	60	6.0	6.2	6.0	95	91	91	-8.3	-7.8	-7.9	2.2	1.3	1.5
	70	4.9	4.9	4.9	104	110	114	-6.7	-5.8	-5.3	4.4	2.8	1.9
	90	5.1	0.6	3.7	112	176	142	-6.1	-2.1	-3.9	6.8	4.7	1.5
Bend angle (50 mm top)	0	7.2	7.5	7.7	88	83	80	-11.	-12.	-13.	3.0	2.6	2.0
	15	7.3	7.6	7.9	82	75	73	-12.	-13.	-14.	1.2	1.5	2.5
	30	7.0	7.4	7.9	79	77	69	-12.	-12.	-13.	1.6	2.4	3.4
	45	7.3	7.5	7.8	83	79	73	-10.	-11.	-12.	1.1	1.5	1.9
	60	7.1	6.8	7.1	87	81	87	-9.7	-9.4	-10.	1.0	1.1	1.3
	70	6.9	6.8	6.9	83	87	81	-9.4	-5.4	-4.5	2.5	2.9	2.0
	90	6.5	5.8	5.1	89	99	110	-8.9	-7.2	-6.4	5.6	12.6	10.3

Table 4. Results for the drooped microstrip, substrate permittivity 2.2.

ε_r=4.2		Bore-sight gain (dBi)			3 dB Beamwidth (deg)			Near horizon gain Roll-off (dB)			RMS phase error (deg)		
Width-mm		60	80	100	60	80	100	60	80	100	60	80	100
Bend angle (30 mm top)	0	4.7	5.8	6.2	114	106	100	-11.	-14.	-14.	1.6	1.2	1.1
	15	6.6	7.0	7.5	89	81	75	-8.4	-9.4	-11.	0.8	1.0	1.7
	30	5.1	5.4	5.6	106	102	93	-7.8	-8.6	-9.4	4.2	3.8	4.7
	45	5.6	6.0	6.4	91	89	83	-7.1	-7.4	-8.1	2.1	2.0	2.6
	60	4.5	4.9	5.1	102	104	100	-7.7	-7.3	-7.3	5.2	3.9	3.8
	70	3.4	4.2	4.3	114	110	118	-7.2	-6.1	-5.0	5.0	2.7	1.6
	90	4.7	4.7	4.4	102	100	110	-6.7	-6.0	-5.1	2.5	2.1	1.4

Table 5. Results for the drooped microstrip, substrate permittivity 4.2.

http://dx.doi.org/10.5772/55002

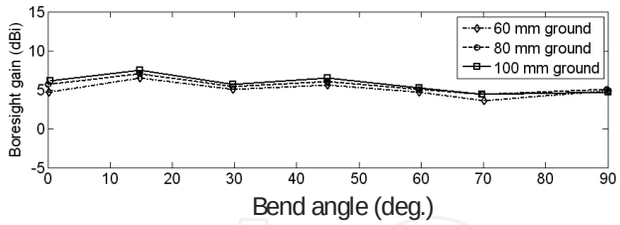

Figure 19. Gain variation with upward bend angle for three ground plane sizes, $\varepsilon_r = 4.2$. (Bend forming a 30 mm flat center section).

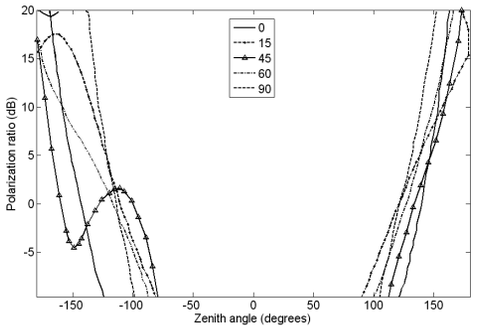

Figure 20. Cross polarization rejection (Defined as the ratio of the cross-polarized to the co-polarized components) for different bend angles (0^0, 15^0, 45^0, 60^0, and 90^0), 100 mm ground plane, $\varepsilon_r = 2.2$.

4. Concluding remarks

In this chapter, we have presented numerical simulations and experimental measurements to analyze downward and upward drooped microstrip antennas with the intent of modifying the radiation pattern of the basic planar patch to accommodate the coverage requirements of GPS marine navigation and positioning. Magnitude and phase of the simulated and measured far-field radiation patterns are presented to reveal the tradeoffs in performance between patch geometry, ground plane size, and orientation. Results reported for the wide range of structural variations applied to the base antenna along with changes in the substrate material should be valuable to designers seeking to achieve a specific coverage performance.

It has been found that an accurate and stable phase center can be obtained over the entire hemisphere for moderate upward bends. Numerical simulations and measurements demonstrate that the 3-dB beamwidth of the flat microstrip patch can be increased by at least 15% and 60% for the downward and upward bends, respectively. The phase stability demonstrated by the slightly bent structures may be viewed as advantageous in cases where circumstances require distorting the element but where a significant alteration in the pattern is not desired. These were accomplished, however, at the expense of some loss of the low-profile character of the antenna.

Although not dramatically affected, the cross polarization discrimination of the bent antennas is reduced by 3 dB at the horizon compared to the equivalent flat case. Calculations of the RMS error in the spherical phase fit over the upper hemisphere showed little change with bend angle or position. In general, there is a tradeoff in achieving broad-beam pattern coverage, and maintaining high cross polarization discrimination.

The crossed dipole source, when used with the pedestal ground plane, demonstrated significant pattern improvements which inspired our interest in the drooped microstrip structure. It should be noted, however, that the crossed dipole is fundamentally different from the microstrip antenna, being itself a stand-alone radiator which operates in the presence of secondary sources created by the ground plane image. For the microstrip antenna, the ground plane is an integral part of the structure. The interior field distribution of the fundamental mode remains essentially unchanged with ground plane manipulation, and pattern modification can come about only by repositioning of the radiating edges in space.

Author details

Ken G. Clark[1], Hussain M. Al-Rizzo[2*], James M. Tranquilla[1], Haider Khaleel[3] and Ayman Abbosh[2]

*Address all correspondence to: hmalrizzo@ualr.edu

1 EMR Microwave Technology Corporation, 64 Alison Blvd., Fredericton, NB, Canada

2 Systems Engineering Department, Donaghey College of Engineering and Information Technology, University of Arkansas at Little Rock, USA

3 Department of Engineering Science, Sonoma State University, Rohnert Park, CA, USA

References

[1] Wells, D. Editor), Guide to GPS Positioning, Larry D Hothem, December (1986).

[2] Ho, C. H, Shumaker, P. K, Fan, L, Smith, K. B, & Liao, J. W. Printed Cylindrical Slot Antenna for GPS Commercial Applications. *Electron. Lett*., Feb. (1996). , 32, 151-152.

[3] Ho, C. H, Shumaker, P. K, Fan, L, Smith, K. B, & Liao, J. W. A Novel GPS Avionics Antenna. *IEEE Antennas Propagat. Lett*., (1996). , 1950-1953.

[4] Altshuler, E. E. Hemispherical Coverage Using a Double-Folded Monopole. *IEEE Trans. Antennas Propagat*., Aug. (1996). , 44(8), 1112-1119.

[5] Ying, Z, & Kildal, P. S. Improvement of Dipole, Helix, Spiral, Microstrip Patch and Aperture Antennas with Ground Planes by Using Corrugated Soft Surfaces. *IEE Proc. Microw. Antennas Propagat*., Jun. (1996). , 143(3), 244-248.

[6] Pozar, D. M, Duffy, S. M, & Dual-band, A. Circularly Polarized Aperture-Coupled Stacked Microstrip Antenna for Global Positioning Satellite. *IEEE Trans. Antennas Propagat*., Nov. (1997). , 45(11), 1618-1625.

[7] Padros, N, Ortigosa, J. I, Baker, J, Iskander, M. F, & Thornberg, B. Comparative Study of High-Performance GPS Receiving Antenna Designs. *IEEE Trans. Antennas Propagat*., Apr. (1997). , 45(4), 698-706.

[8] Kan, H. K, Waterhouse, R. B, & Small, A. CP-Printed Antenna Using 120 deg Sequential Rotation. *IEEE Trans. Antennas Propagat*., Mar. (2002). , 50(3), 398-399.

[9] Lee, S, Woo, J, Ryu, M, & Shin, H. Corrugated Circular Microstrip Patch Antennas for Miniaturization. *Electron. Lett*., Mar. (2002). , 38, 262-263.

[10] Boccia, J. L, & Amendola, G. and G. Di Massa. A Shorted Elliptical Patch Antenna for GPS Applications. *IEEE Antennas Wireless Propagat. Lett.*, (2003). , 2, 6-8.

[11] Ozgun, O, Mutlu, S, Aksun, M. I, & Atalan, L. Design of Dual-Frequency Probe-Fed Microstrip Antennas with Genetic Optimization Algorithm. *IEEE Trans. Antennas Propagat*., Aug. (2003). , 51(8), 1947-1954.

[12] Boccia, L, Amendola, G, & Massa, G. D. A Dual Frequency Microstrip Patch Antenna for High-Precision GPS Applications. *IEEE Antennas Propagat. Lett*., (2004). , 3, 157-160.

[13] Oh, K, Kim, B, & Choi, J. Novel Integrated GPS/RKES/PCS Antenna for Vehicular Application. *IEEE Microwave Wireless Comp. Lett*., Apr. (2005). , 15(4), 244-246.

[14] Basilio, L. I, Williams, J. T, Jackson, D. R, & Khayat, M. A. A Comparative Study of a New GPS Reduced-Surface-Wave Antenna. *IEEE Antennas Propagat. Letters*, (2005). , 4, 233-236.

[15] Zhang, Y, & Hui, H. T. A Printed Hemispherical Helical Antenna for GPS Receivers. *IEEE Microwave and Wireless Comp. Lett*., January (2005). , 15(1), 10-12.

[16] Azaro, R, De Natale, F, Donelli, M, Zeni, E, & Massa, A. Synthesis of a Prefractal Dual-Band Monopolar Antenna for GPS Applications," *IEEE Antennas Wireless Propagat. Lett.*, (2006). , 5, 361-364.

[17] Zhou, Y, Koulouridis, S, Kiziltas, G, Volakis, J. L, & Novel, A. Quadruple Antenna for Tri-Band GPS Applications. *IEEE Antennas Wireless Propagat. Lett*., (2006). , 5, 224-227.

[18] Basilio, L. I, Chen, R. L, Williams, J. T, & Jackson, D. R. A New Planar Dual-Band GPS Antenna Designed for Reduced Susceptibility to Low-Angle Multipath. *IEEE Trans. Antennas Propagat*., Aug. (2007). , 55(8), 2358-2366.

[19] Boccia, L, Amendola, G, & Massa, G. D. Performance Evaluation of Shorted Annular Patch Antennas for High-Precision GPS Systems. *IET Microwave Antennas Propagat*., (2007). , 1(2), 465-471.

[20] Zhou, Y, Chen, C. C, & Volakis, J. L. Dual Band Proximity-Fed Stacked Patch Antenna for Tri-Band GPS Applications. *IEEE Trans. Antennas Propagat*., Jan. (2007). , 55(1), 220-223.

[21] Lachapelle, G, Casey, M, Eaton, R. M, Kleusberg, A, Tranquilla, J, & Wells, D. GPS Marine Kinematic Positioning Accuracy and Reliability. *The Canadian Surveyor*, Summer (1987). , 41(2), 143-172.

[22] Lachapelle, G, Liu, C, Lu, G, Cannon, M. E, Townsend, B, & Hare, R. Precise Marine DGPS Positioning Using P Code and High Performance C/A Code Technologies. *National Technical Metting, ION*, San Francisco, Jan. (1993).

[23] Yaesh, I, & Priel, B. Design of Leveling Loop for Marine Navigation System. *IEEE Trans. Aerospace Electr. Sys.*, Apr. (1993). , 29(2), 599-604.

[24] Deifes, D. GPS Based Attitude Determining System for Marine Navigation. *IEEE Position, Location, and Navigation Symposium*, Apr. (1994). , 806-812.

[25] Lachapelle, G, Cannon, M. E, Lu, G, & Loncarevic, B. Ship borne GPS Attitude Determination During MMST-93. *IEEE J. Oceanic Eng.*, Jan. (1996). , 21(1), 100-105.

[26] Shumaker, P. K, Ho, C. H, & Smith, K. B. Printed Half-Wavelength Quadrifilar Helix Antenna for GPS Marine Applications. *Electron. Lett*., February (1996). , 32, 153-154.

[27] Beiter, S, Poquette, R, Filipo, B. S, & Goetz, W. Precision Hybrid Navigation System for Varied Marine Applications. *IEEE Position, Location, and Navigation Symposium*, April (1998). , 316-323.

[28] Tranquilla, J. M, Carr, J. P, & Al-rizzo, H. M. Analysis of a Choke Ring Ground Plane for Multipath Control in Global Positioning System (GPS) Applications. *IEEE Trans. Antennas Propagat*., Oct. (1994). , 42, 905-911.

[29] Counselman, C. C. III. Multipath-Rejecting GPS Antennas. *Proc. of the IEEE*, Jan. (1999). , 87(1), 86-91.

[30] Townsend, B. R, & Fenton, P. C. A Practical Approach for the Reduction of Pseudorange Multipath Errors in a L1 GPS Receiver. ION-94, Salt Lake City, Sept. (1994). , 1-6.

[31] Tranquilla, J. M. The Experimental Study of Global Positioning Satellite Antenna Backplane Configurations. Technical Report, NASA Jet Propulsion Lab., Contract 957959, Radiating Systems Research Laboratory, University of New Brunswick, Fredericton, NB, Canada, (1988).

[32] Tranquilla, J. M, Colpitts, B. G, & Carr, J. P. Measurement of Low Multipath Antennas for Topex. Proceedings of the *5th International Geodetic Symposium on Satellite Positioning*, Las Cruces, NM, Mar. 13-1 7, (1989). , 356-361.

[33] Tanquilla, J. M, & Colpitts, B. G. Development of a Class of Antennas for Space-Based NAVSTAR GPS Applications. *International Conference on Antennas and Propagation (ICAP 89)*, 6th, Coventry, England, Apr. 4-7, 1989, Proceedings. Part 1 (A90-27776 11-32). London, England and Piscataway, NJ, Institution of Electrical Engineers, (1989). , 65-69.

[34] Tranquilla, J. M, & Colpitts, B. G. GPS Antenna Design Characteristics for High Precision Applications. Proceedings of the *ASCE Conference GPS-88 Engineering Applications of GPS Satellite Surveying Technology*, Nashville, TN, May (1988). , 11-14.

[35] Tranquilla, J. M, & Best, S. R. A Study of the Quadrifilar Helix Antenna for Global Positioning Systems (GPS) Applications. *IEEE Trans. Antennas Propagat*., Oct.(1990). , 38, 1545-1550.

[36] Noghanian, S, & Shafai, L. Control of Microstrip Antenna Radiation Characteristics by Ground Plane Size and Shape. *IEE Proc. Microw. Antennas Propagat*., Ju.(1998). , 145, 207-212.

[37] Clark, K. G. The Finite-Difference Time-Domain Technique Applied to the Drooped Microstrip Antenna. PhD thesis, Department of Electrical Engineering, University of New Brunswick, Fredericton, NB, Canada, Jul. (1996).

[38] Feller, W. Three Dimensional Microstrip Patch Antenna. US Patent Publication Apr. (1993). (5)

[39] Su, C. W, Huang, S. K, & Lee, C. H. CP Microstrip Antenna with Wide Beamwidth for GPS Band Application. *Electronics Lett*., th Sept. (2007). , 43(20)

[40] Colpitts, B. G. The Uniform Theory of Diffraction Applied to Wedges and Curved Surfaces. PhD thesis, Department of Electrical Engineering, University of New Brunswick, Fredericton, NB, Canada, Apr.(1988).

[41] Taflove, A, & Umashankar, K. R. Finite-Difference Time-Domain Modeling of Electromagnetic Wave Scattering and Interaction Problems. *IEEE Trans. Antennas Propagat. Society Newslett*., Apr. (1988). , 5-20.

[42] Jurgens, T. G, Taflove, A, Umashankar, K. R, & Moore, T. G. Finite-Difference Time-Domain Modeling of Curved Surfaces. *IEEE Trans. Antennas Propagat*., Apr. (1992). , AP-40, 357-366.

[43] Tranquilla, J. M, & Best, S. R. Phase Center Considerations for the Monopole Antenna. *IEEE Trans. Antennas Propagat*., May (1986). , AP-34, 741-744.

IntechOpen

IntechOpen